

1 **Editor summary:**

2 The formation of continental crust may have trapped – and thus not degassed - substantial magmatic nitrogen over Earth’s history, according to  
3 geochemical analyses of igneous rocks from the Hekla volcanic system in Iceland.

4

5 **Peer Review Information:**

6 Primary handling editors: Tamara Goldin and Rebecca Neely, in collaboration with the Nature Geoscience team.

7 *Nature Geoscience* thanks Tobias Fischer, Ralf Halama, Olgeir Sigmarrsson and the other, anonymous, reviewer(s) for their contribution to the peer review of  
8 this work.

9

10

11 **1. Supplementary Information:**

12 **A. PDF Files**

Item	Present?	Filename  Whole original file name including extension. i.e.: Smith_SI.pdf. The extension must be .pdf	A brief, numerical description of file contents.  i.e.: <i>Supplementary Figures 1-4, Supplementary Discussion, and Supplementary Tables 1-4.</i>
Supplementary Information	Yes	Boocock et al_Hekla Supplement.pdf	Supplementary Figures 1-6 and Supplementary Discussion

13

14

15

## B. Additional Supplementary Files

Type	Number Each type of file (Table, Video, etc.) should be numbered from 1 onwards. Multiple files of the same type should be listed in sequence, i.e.: Supplementary Video 1, Supplementary Video 2, etc.	Filename Whole original file name including extension. i.e.: <i>Smith_Supplementary_Video_1.mov</i>	Legend or Descriptive Caption Describe the contents of the file
Supplementary Data	1	Data_Hekla All Data.xlsx	Spreadsheet
Supplementary Data	2	Data_Felsic N Compilation.xlsx	Spreadsheet

16

17

18

## 3. Source Data

Parent Figure or Table	Filename Whole original file name including extension. i.e.: <i>Smith_SourceData_Fig1.xls</i> , or <i>Smith_Unmodified_Gels_Fig1.pdf</i>	Data description i.e.: Unprocessed western Blots and/or gels, Statistical Source Data, etc.
Source Data Fig. 1	Data_Hekla All Data.xlsx	Geochemical Data
Source Data Fig. 2	Data_Hekla All Data.xlsx	Geochemical Data
Source Data Fig. 3	Data_Hekla All Data.xlsx	Geochemical Data
Source Data Extended Data Fig./Table 1	Data_Hekla All Data.xlsx	Geochemical Data
Source Data Extended Data Fig./Table 2	Data_Hekla All Data.xlsx	Geochemical Data

Source Data Extended Data Fig./Table 3	Data_Hekla All Data.xlsx	Geochemical Data
Source Data Extended Data Fig./Table 4	Data_Hekla All Data.xlsx	Geochemical Data
Source Data Extended Data Fig./Table 5	Data_Hekla All Data.xlsx	Geochemical Data

19

20

21 **A primary magmatic source of nitrogen to the Earth's crust**

22

23 Toby J. Boocock<sup>1,\*</sup>, Sami Mikhail<sup>1</sup>, Adrian J. Boyce<sup>2</sup>, Julie Prytulak<sup>3</sup>, Paul S.  
24 Savage<sup>1</sup>, Eva E. Stüeken<sup>1</sup>

25

26 <sup>1</sup>*School of Earth & Environmental Sciences, University of St Andrews, KY16 9AL, UK*

27 <sup>2</sup>*Scottish Universities Environmental Research Centre, Rankine Avenue, East Kilbride, G75*  
28 *0QF, UK*

29 <sup>3</sup>*School of Earth Sciences, University of Durham, Durham, DH1 3LE, England, UK*

30

---

31 \*Corresponding Author: [tjb7@st-andrews.ac.uk](mailto:tjb7@st-andrews.ac.uk)

32

33 **ORCID IDs**

34 Toby J. Boocock - [0000-0003-0452-4824](https://orcid.org/0000-0003-0452-4824)

35 Sami Mikhail - [0000-0001-5276-0229](https://orcid.org/0000-0001-5276-0229)

36 Adrian J. Boyce - [0000-0002-9680-0787](https://orcid.org/0000-0002-9680-0787)

37 Julie Prytulak - [0000-0001-5269-1059](https://orcid.org/0000-0001-5269-1059)

38 Paul S. Savage - [0000-0001-8464-0264](https://orcid.org/0000-0001-8464-0264)

39 Eva E. Stüeken - [0000-0001-6861-2490](https://orcid.org/0000-0001-6861-2490)

40 **The igneous portion of Earth's continental crust represents a long-term sink of terrestrial**  
41 **nitrogen, but the origin of the nitrogen in this reservoir remains ambiguous. Possible**  
42 **sources include magmatic differentiation of mantle-derived melts (i.e., magmatic nitrogen)**  
43 **and/or the burial of biomass (i.e., fixed atmospheric nitrogen). Identifying the source of**  
44 **crustal nitrogen is required to accurately reconstruct the evolution of Earth's atmospheric**  
45 **pressure, and therefore habitability, over geologic timescales. Here we present analyses of**  
46 **the nitrogen geochemistry of extrusive igneous rocks from Hekla volcano, Iceland, that has**  
47 **been previously used as a natural laboratory to study the effects of magmatic**  
48 **differentiation on stable isotope systems. We find that bulk rock nitrogen abundance**  
49 **increases as rocks become more evolved, with up to 23  $\mu\text{g/g}$  of nitrogen in felsic igneous**  
50 **samples, with non-systematic and negligible nitrogen isotopic fractionation across the**  
51 **suite. Our findings support nitrogen that is magmatic in origin and that behaves as an**  
52 **incompatible trace element during magmatic differentiation. Assuming Hekla is**  
53 **representative of differentiating systems more broadly, the observed nitrogen enrichment**  
54 **would satisfy 31-52% of Earth's felsic crust-hosted nitrogen. We suggest that continental**  
55 **crust formation can act as nitrogen trap between the mantle and the atmosphere.**  
56 **Therefore, nitrogen degassing from Earth's interior to the atmosphere over geological time**  
57 **may have been previously overestimated.**

58         The mass and composition of Earth's atmosphere are crucial variables for maintaining  
59 habitability over billion-year timescales, and yet one critical parameter remains poorly  
60 constrained: the long-term evolution of atmospheric pressure<sup>1,2</sup>. Conservation of mass  
61 requires that changes in one reservoir (i.e., the atmosphere, where nitrogen is the major  
62 contributor of total pressure) must be balanced by reciprocal changes in other reservoirs (i.e.,  
63 the crust or mantle). As such, the processes that cycle nitrogen between these reservoirs need  
64 to be constrained in order to understand the processes that enrich this bio-essential element  
65 on planetary surfaces<sup>2</sup>. The atmosphere and mantle are the largest nitrogen reservoirs, and  
66 they dynamically exchange nitrogen via subduction zone plate tectonics and volcanism<sup>3,4</sup> (Fig.  
67 1a). Between them is a third reservoir, Earth's continental crust. The crust is important as it  
68 stores roughly half as much nitrogen as the present-day atmosphere<sup>1</sup>. Although lithologically  
69 heterogeneous, around 50% of the Earth's upper crust is of felsic igneous composition,  
70 making magmatic differentiation an important process during crust formation. These felsic  
71 igneous rocks can contain up to ca. 250  $\mu\text{g/g}$  nitrogen<sup>1</sup> (Fig 1b), and with residence times of  
72 over 1000 Myr they offer potential as long term stores of nitrogen and as a key substrate for  
73 the development and evolution of life.

74         The upper crustal igneous reservoir can have two primary nitrogen sources: anatexis  
75 of nitrogen-enriched sediments (i.e., burial, diagenesis, partial melting), and magmatic  
76 differentiation of effectively mantle-derived nitrogen. The former would mean that the felsic  
77 igneous nitrogen reservoir was derived predominantly from the atmosphere via biomass  
78 burial, implying that this amount of nitrogen was once part of the atmospheric  $\text{N}_2$  budget. In  
79 contrast, magmatic enrichment would imply the exact opposite, meaning that crustal  
80 differentiation can act as a trap for mantle nitrogen and thereby limit volcanically degassed  
81 atmospheric  $\text{N}_2$  accumulation.

82 To address the origin of Earth's felsic igneous nitrogen reservoir, we have determined  
83 the nitrogen geochemistry for a suite of well-characterised<sup>8-17</sup> volcanic igneous samples from  
84 Hekla volcano, Iceland. Hekla is an active volcanic system situated in the South Iceland  
85 Volcanic Zone that produces a range of extrusive igneous rocks spanning the tholeiitic  
86 magmatic series (Fig. 2a), manifesting as aphyric lavas and tephra. Eruptions span historical  
87 timescales with 18 eruptions since 1104 A.D and the most recent activity in 2000 A.D.<sup>8</sup>.  
88 Eruptions typically began explosively (Si-rich), followed by later effusive (Si-poor) behaviour  
89 with the degree of Si enrichment being related to the repose time of magma storage<sup>8</sup>. Our  
90 samples are phenocryst-poor (containing << 5% of plagioclase, pyroxene, titanomagnetite,  
91 olivine and apatite<sup>9</sup>). The source of primary magmas at Hekla are estimated to come from 17-  
92 28 km depths<sup>11</sup> and represent melts derived by ca. 10% partial melting of the Icelandic  
93 mantle<sup>17</sup>. There remains debate surrounding the petrogenesis of differentiated Hekla rocks.  
94 One view is that Hekla samples are a cogenetic magmatic suite produced by variable degrees  
95 of fractional crystallisation of mantle-derived basaltic melt; broadly, this model is based on  
96 the fact that, for all Hekla samples, many major and trace element tracers of fractional  
97 crystallisation plot on a single liquid line of descent with limited evidence for crustal  
98 assimilation<sup>8</sup>. However, this simple model does not seem to agree with evidence from U-  
99 series isotopes and associated trace-element (e.g. Th) systematics; broadly, these models  
100 imply that it is only Hekla basaltic andesites that are derived from the fractionation  
101 crystallisation of mantle melts, and that partial melting of basaltic rocks (i.e. older Icelandic  
102 crust) is required to generate the dacites and rhyolites (the andesites are formed from mixing  
103 between these two melt sources)<sup>10,12,20</sup>. Therefore, it is conceivable that Hekla erupts material  
104 that has experienced fractional crystallisation, partial melting and/or magma mixing of two  
105 distinct sources (mantle and hydrated mafic crust)<sup>17</sup>.

106 Hekla has been successfully used as a natural laboratory to study of the effect of  
107 magmatic differentiation *sensu lato* on many stable isotope systems (O, Ti, Li, Fe, Si, K, Zr, Mo,  
108 V, Zn)<sup>9-10,13-20</sup>. Importantly, for most of these isotope systems, their variations (or lack thereof)  
109 at Hekla can be explained well with either model of petrogenesis. Furthermore, the  
110 systematics of stable isotope fractionation in Hekla rocks are comparable to that measured in  
111 other geologically distinct systems (e.g. Kīlauea, Hawaii<sup>15-16,18</sup> and Anatahan, Mariana  
112 Islands<sup>15-16</sup>), suggesting that Hekla is not a special case, but provides samples representative  
113 of a differentiating system. For the case of nitrogen, its chemical behaviour best matches that  
114 of the large ion lithophile elements (LILE) at Hekla (see later). These elements can be modelled  
115 using a simple fractional crystallisation model and so initially we follow this approach for  
116 nitrogen. However, we acknowledge, and discuss, the effect that the more complicated  
117 petrogenesis model has on nitrogen and its isotopes and conclude that application of either  
118 model does not significantly affect our conclusions.

119 We selected and measured 17 replicate (n = 2 to 4) Hekla samples (Supplementary  
120 table S1) for their bulk rock nitrogen abundance and stable isotope compositions ( $\delta^{15}\text{N} =$   
121  $[(^{15}\text{N}/^{14}\text{N})_{\text{sample}} / (^{15}\text{N}/^{14}\text{N})_{\text{air}} - 1] \times 1000$ ), using a custom-built sealed tube combustion line<sup>21</sup>.  
122 These data represent total nitrogen hosted in the silicate. This is inclusive of – not limited to  
123 – nitrogen bound in silicate lattices and nitrogen dissolved in the structure of a glass (formerly,  
124 melt) and should not be confused with N<sub>2</sub> measurements liberated from *in-vacuo* crushing of

125 fluid or gas inclusions, where the measured  $N_2$  (gas phase) is less than  $N^{\text{total}}$ . As is well established,  
126 nitrogen is incorporated into silicates systems (crystals, melt, fluids) as multiple molecular  
127 species (e.g.,  $N_2$ ,  $NH_3$ ,  $NH_4^+$ ,  $N^{3-}$ )<sup>22–24</sup> both lattice-bound and as impurities. As such, our bulk  
128 combustion methodology *sensu stricto* measures total silicate nitrogen. Bulk rock stable  
129 oxygen isotope values ( $\delta^{18}O = [(^{18}O/^{16}O)_{\text{sample}} / (^{18}O/^{16}O)_{\text{VSMOW}} - 1] \times 1000$ ) were also measured  
130 by laser fluorination as a tracer for crustal assimilation and alteration (see Methods and  
131 supplementary material, Fig.S1-2). Major and trace element abundances and published  
132 isotope values were compiled from previous studies<sup>8–10,13,20</sup>. Our data show an eight-fold  
133 increase in nitrogen abundance as the rocks become more evolved (Fig 2b) from ca. 3  $\mu\text{g/g}$  in  
134 the basalt samples to ca. 23  $\mu\text{g/g}$  in the rhyolite samples with no systematic fractionation of  
135 nitrogen isotopes across the suite (averaging  $\delta^{15}N = +1.3 \pm 1.8\text{‰}$ ; fig 2c) and, for most  
136 samples, no deviation in geochemical behaviour between nitrogen and the large ion lithophile  
137 elements (LILEs, such as rubidium; fig 2b,d).

### 138 **The Origin of Nitrogen Enrichment at Hekla**

139 We posit that the nitrogen systematics at Hekla are best explained by nitrogen  
140 behaving as an incompatible trace element during magmatic differentiation. The enrichment  
141 in nitrogen abundance between the basaltic and rhyolitic samples (Fig.2b) cannot be  
142 explained by degassing or late-stage fluid alteration. Our data show no systematic  
143 fractionation of nitrogen isotope values from basalt to rhyolite (Fig 2c), and we note that the  
144 variability for observed  $\delta^{15}N$  values are within the range documented for the Icelandic mantle  
145 plume<sup>25</sup> ( $\delta^{15}N = -2.29$  to  $+5.71\text{‰}$ ). The constancy of the  $\delta^{15}N$  value (averaging  $\delta^{15}N = +1.3 \pm$   
146  $1.8\text{‰}$ ) relative to silica (Fig.2c) is consistent with small magnitude equilibrium stable isotope  
147 fractionation at high temperature<sup>31</sup> and generally inconsistent with the loss or gain of  
148 nitrogen from interaction with fluids<sup>29</sup>. This lack of alteration is in agreement with previously  
149 published radiogenic<sup>8,10,20</sup> and stable<sup>9,13,14,16–19</sup> isotope datasets for Hekla volcanics (more  
150 information is provided in the supplementary material, sections S1.3 and S1.4). Our  $\delta^{18}O$   
151 values show a slight increase between  $+4.0$  to  $+5.0\text{‰}$  as a function of melt evolution (Fig.S1),  
152 and this general increase in  $\delta^{18}O$  of ca.  $+1\text{‰}$  as the system evolves is fully consistent with  
153 equilibrium fractional crystallisation of basalt to rhyolite in tholeiitic systems<sup>30</sup>. We can  
154 therefore rule out secondary sources of nitrogen as the control on the relative enrichment of  
155 nitrogen in the evolved units relative to the mafic lavas.

156 In a system where degassing was the dominant driver for nitrogen geochemistry one  
157 would predict the evolved lithologies (dacites and rhyolites) to be depleted in nitrogen  
158 abundance relative to the more mafic samples (basaltic and andesitic) due to progressive loss  
159 of a volatile component, but we observe the opposite (Fig. 2b). The lack of significant nitrogen  
160 degassing is further supported by the constancy of the N/Rb ratio across the sample suite (Fig.  
161 2d). Moreover, the N/Rb of our samples are well below the range expected for  
162 hydrothermally sourced nitrogen (Fig. 2d) and suggests a behavioural coupling of nitrogen  
163 and rubidium as the magmatic system evolves. Since rubidium concentrations exhibit typical  
164 non-volatile incompatible trace element behaviour in Hekla eruption products (Fig 2b –  $r^2 =$   
165  $0.99$ , rubidium vs barium), the invariance of the N/Rb ratio between the basalts and rhyolites  
166 suggests that, in the Hekla volcanic system, nitrogen is behaving in the same manner to a LILE.

167 We have modelled the effect of degassing on N/Rb if nitrogen were lost to a gas phases  
168 (volatile behaviour where  $D_{N \text{ fluid-melt}} = 60\text{-}10000$ , ref <sup>29</sup>) whilst rubidium was not (lithophile  
169 behaviour where  $D_{Rb \text{ mineral-melt}} = 0.001$ ). The estimate for the N-partition coefficient is valid for  
170 highly reduced ( $fO_2 < IW$ ) to highly oxidised ( $fO_2 > NNO$ ) systems of both basaltic ( $D_{N \text{ fluid-melt}} =$   
171  $10,000$ ) and felsic ( $D_{N \text{ fluid-melt}} = 60$ ) compositions. Taking even the most conservative values  
172 ( $D_{N \text{ fluid-melt}} = 60$ ), and assuming 100% degassing, we find that the molar N/Rb ratio would  
173 rapidly decrease, which is inconsistent with these data. The maximum amount of volatile  
174 nitrogen that the model permits is 1-5% ( $D_{N \text{ fluid-melt}} = 0.6\text{-}3$ ), and this may explain the slight  
175 dip in N/Rb observed between the basalts and basaltic andesites (Fig. 2d), but fails to satisfy  
176 the plateau in nitrogen abundance between the same samples in nitrogen versus barium  
177 space (Fig.2b) when rubidium and barium are positively correlated throughout the suite  
178 (Fig.S3). Collectively, these data require that > 95% of nitrogen behaved as an incompatible  
179 lithophile element. Importantly, these calculations were performed with a conservative fluid-  
180 melt partition coefficient for felsic melts as a baseline value to represent 100% degassing ( $D_{N$   
181  $\text{fluid-melt}} = 60$ ). If instead we use the partition coefficients for basaltic melts ( $D_{N \text{ fluid-melt}} = 10,000$ ),  
182 then only 0.006-0.03% of the total nitrogen could have behaved as a volatile element to fit  
183 these data.

184 The isotope data also support a model where nitrogen is retained and not degassed.  
185 If degassing was the key control on the nitrogen geochemistry of this system then one might  
186 predict modification of the primary  $^{15}N/^{14}N$  of the melt resulting in progressive  $^{15}N$   
187 enrichment<sup>26</sup> following Rayleigh degassing trend(s)<sup>32</sup>. It is worth noting, however, that some  
188 previous studies have found limited fractionation (< 1 to 2‰) of nitrogen isotopes between  
189 olivine fluid inclusion hosted nitrogen liberated by *in-vacuo* crushing and geothermal gasses  
190 from the same volcanic systems<sup>33</sup>, whereas others have noted significant resolvable isotopic  
191 fractionation associated with degassing<sup>26</sup>. Therefore, although lack of isotopic fractionation  
192 alone is not definitive, we argue that the combined 8-fold enrichment in nitrogen abundance  
193 alongside the lack of resolvable fractionation for N/Rb and  $^{15}N/^{14}N$  are inconsistent with  
194 degassing being the major control over nitrogen geochemistry on Hekla. Hence any nitrogen  
195 degassing that did occur was very minor (<5%) relative to the amount of nitrogen that was  
196 retained by the melt (>95%).

197 Up to now we have considered that fractional crystallisation is the major igneous  
198 process causing magmatic differentiation on Hekla. If we instead follow the model wherein  
199 the dacites and rhyolites are generated via partial melting of basaltic Icelandic crust and  
200 subsequent fractional crystallisation<sup>12</sup>, we find that this generates nitrogen compositions that  
201 plot on arrays that are co-linear with rubidium and caesium (Fig 2b); that is, they plot on the  
202 same liquid line of descent that would be predicted if fractional crystallisation of the basalt  
203 generated the magmatic suite on Hekla. Therefore, in terms of igneous processes, partial  
204 melting of older hydrated Icelandic basalts generates melts with nitrogen concentrations that  
205 would be predicted if nitrogen was behaving as an incompatible LILE, and not a volatile  
206 element. One argument is that the remelting of (hydrated) basaltic crust could be sampling  
207 source rocks that have had secondary nitrogen enrichment; however, the consistency of our  
208 nitrogen isotope data, as well as the lack of evidence for assimilation of non-igneous sources  
209 on Hekla<sup>8</sup> (e.g. a linear relationship between Li vs SiO<sub>2</sub>; Fig S2; consistency of Li and Tl isotope



210 compositions across the Hekla suite<sup>13,16</sup>) implies that all the nitrogen sampled at Hekla is  
211 igneous in origin. To explain the nitrogen concentrations in the basaltic andesites and  
212 andesites in terms of this more complicated petrological model, small amounts of nitrogen  
213 degassing could have occurred when the mantle-derived basalt differentiated to form the  
214 basaltic andesites. The array of nitrogen concentrations in the andesites could then be  
215 generated via mixing between relatively N-rich dacitic and rhyolitic melts, and the partially  
216 degassed basaltic andesite melt, leading to andesites which have the widest range of nitrogen  
217 concentrations. This is consistent with the data (Fig 2b) and resulting in what appears to be  
218 an unbroken cogenetic relationship between basaltic andesites and rhyolites at Hekla<sup>12</sup>.

219 To summarise, the behaviour of nitrogen and its isotopes in Hekla samples is  
220 consistent with whichever petrological model is accepted (e.g., Ref 8 vs Ref 12). Furthermore,  
221 we infer that all nitrogen in Hekla rocks is ultimately magmatic in origin, and we posit that in  
222 an undersaturated magma, nitrogen exhibits similar behaviour to the incompatible element  
223 rubidium, a large ion lithophile, and is progressively enriched during magmatic differentiation.

#### 224 **A Mantle Source for Crustal Nitrogen**

225 The lack of evidence for volatile behaviour during magmatic differentiation at Hekla  
226 has important implications for Earth's geological nitrogen cycle. Our data show that nitrogen  
227 can behave like an incompatible element comparable to the LILEs (Rb, Cs) during magmatic  
228 differentiation, possibly spanning the whole tholeiitic magma series, but certainly applicable  
229 to when a lower crustal hydrated basalt partially melts to form a dacite or rhyolite, with a bulk  
230 partition coefficient ( $D_{N \text{ mineral-melt}} \ll 1$ ). Importantly, the process of lower crustal anatexis via  
231 dehydration melting of meta-mafic rocks is how I-type granites (granites with dominantly  
232 igneous source rocks) are formed. Our data suggest that when the system is nitrogen  
233 undersaturated, nitrogen should not be considered a strictly volatile element during  
234 magmatic differentiation. To extrapolate our results to global average crust, we can therefore  
235 treat nitrogen as a highly incompatible trace element (Fig. 3). We chose the trace element  
236 barium as a differentiation proxy since it is highly incompatible ( $r^2=0.99$ , Ba vs SiO<sub>2</sub>) in the  
237 Hekla system (Fig. 2b). Due to a paucity of relevant partitioning data for systems similar to  
238 Hekla, we assume  $D_{N \text{ mineral-melt}}$  value of 0.001 for nitrogen in our model (see Supplementary  
239 material, S1.5). The best fit model for our data requires a maximum  $D_{N \text{ mineral-melt}}$  of 0.01, below  
240 which variation in  $D_{N \text{ mineral-melt}}$  has negligible impact on the calculated slope.

241

242 Taking average values and uncertainties for the bulk rubidium concentration in the  
243 middle continental crust (MCC) and upper continental crust (UCC)<sup>34</sup> and propagating those to  
244 a fractional crystallisation model for nitrogen versus rubidium allows us to estimate the  
245 amount of nitrogen enrichment that is possible during magmatic differentiation in the  
246 formation of typical mantle-derived rocks in the continental crust. Here we choose rubidium  
247 as it is an incompatible trace element that is expected to partition similarly to nitrogen in  
248 igneous materials due to the similar ionic charge and radius of Rb<sup>+</sup> and NH<sub>4</sub><sup>+</sup> ions. This  
249 estimate does assume that in both cases nitrogen and rubidium are fully behaving as  
250 lithophile elements, and that the average rubidium content of the MCC and UCC are

251 representative of the concentration obtained by magmatic differentiation. Varying  
252 proportions of sediments may impact the rubidium concentration estimates, particularly in  
253 the UCC estimates, whereas previous studies suggest that the average rubidium content of  
254 the felsic crust (ca. 90-150  $\mu\text{g/g}$ )<sup>35</sup> is similar to that of the sedimentary crust (100-200  $\mu\text{g/g}$ )<sup>36</sup>.  
255 As such these are suitable first order estimates of the amount of nitrogen derived by  
256 differentiation. The fractional crystallisation model assumes a basaltic starting composition  
257 with 3.3  $\mu\text{g/g}$  nitrogen (i.e. the abundance measured in the least evolved basaltic sample Hek  
258 06-09), which is consistent with a estimates for mantle plume nitrogen abundances<sup>37</sup>, and  
259 typical of the Icelandic mantle plume<sup>25</sup>. The results of our model suggest that the magmatic  
260 contribution to the felsic igneous crust could amount to 16-19  $\mu\text{g/g}$  (MCC estimate) or 18-27  
261  $\mu\text{g/g}$  (UCC estimate) nitrogen. Taking a total continental crust mass of  $1.9 \times 10^{22}$  kg (ref. 1) and  
262 assuming that 53% of this mass is the UCC<sup>1</sup> and that the UCC is made up of ca. 50% felsic  
263 magmatic rocks<sup>1</sup> we can estimate the mass of nitrogen stored in the continental crust that  
264 may have been derived by magmatic differentiation using the concentration of 16-27  $\mu\text{g/g}$ .  
265 These calculations suggest that between  $8.06 \times 10^{16}$  kg to  $1.36 \times 10^{17}$  kg of nitrogen in the UCC  
266 could be derived from magmatic differentiation of a mantle melts alone. By comparison with  
267 the total mass of nitrogen in the felsic (filtered to >60%  $\text{SiO}_2$  – Fig 1b) UCC ( $2.62 \times 10^{17}$  kg N)<sup>1</sup>,  
268 this represents between 31-52% of felsic-stored nitrogen. For greater context, this mass of  
269 nitrogen is equivalent to the biosphere<sup>1,7,38</sup> and accounts for 5-8% of the estimated total mass  
270 of nitrogen in the total continental crust (if including sediments)<sup>1</sup>. It is worth noting that we  
271 only consider the felsic compositions of the upper continental crust and therefore do not  
272 consider nitrogen contributions from the more mafic lower crust, nitrogen retained in igneous  
273 minerals that are reworked in sediments, or the primary magmatic fraction in metamorphic  
274 rocks not lost during metamorphism. Nevertheless, our results highlight that magmatic  
275 processes alone can enrich nitrogen in the igneous crust. While the (meta-)sedimentary  
276 component of the crust has certainly archived past atmospheric  $\text{N}_2$ , a large proportion of the  
277 felsic igneous nitrogen reservoir is mantle-derived and may never contributed to atmospheric  
278 pressure. In summary, the formation of felsic crusts can act as a nitrogen trap between the  
279 mantle and the atmosphere on Earth and other telluric planets. Therefore, the flux of nitrogen  
280 from Earth's interior to the atmosphere over geological time may have been overestimated<sup>1-  
281 5</sup> because nitrogen is not always lost to degassing during igneous differentiation.

## 282 **Acknowledgements:**

283 Funding was provided by a Natural Environment Research Council studentship (grant  
284 NE/R012253/1) to TJB and a National Environmental Isotope Facility access in-kind grant  
285 (NEIF – 2313.0920) to EES, SM and TJB. SM acknowledges support from NERC standard  
286 grant NE/PO12167/1. EES is financially supported by a NERC Frontiers grant  
287 (NE/V010824/1). We thank Alison MacDonald at SUERC for measuring the bulk oxygen  
288 isotope data.

## 289 **Contributions:**

290 TB, SM, JP and EES designed the study. PSS collected the samples and undertook initial sample  
291 preparation and major/trace element characterisation. TB collected the nitrogen data and  
292 wrote the original manuscript draft. AB collected the oxygen isotope data. All authors

293 contributed to the interpretation of the results and the review and editing of the manuscript  
294 and supplemental information.

295 **Competing interests:**

296 The authors declare no competing interests.

297

## References

- 298 1. Johnson, B. W. & Goldblatt, C. The nitrogen budget of Earth. *Earth-Science Rev.* **148**,  
299 150–173 (2015).
- 300 2. Zerkle, A. L. & Mikhail, S. The geobiological nitrogen cycle: From microbes to the  
301 mantle. *Geobiology* **15**, 343–352 (2017).
- 302 3. Sano, Y. *et al.* Volcanic flux of nitrogen from the Earth. *Chem. Geol.* **171**, 263–271  
303 (2001).
- 304 4. Halama, R., Bebout, G. E., John, T. & Schenk, V. Nitrogen recycling in subducted  
305 oceanic lithosphere: The record in high- and ultrahigh-pressure metabasaltic rocks.  
306 *Geochim. Cosmochim. Acta* **74**, 1636–1652 (2010).
- 307 5. Goldblatt, C. *et al.* Nitrogen-enhanced greenhouse warming on early Earth. *Nat.*  
308 *Geosci.* **2009 212** **2**, 891–896 (2009).
- 309 6. Kerrich, R., Jia, Y., Manikyamba, C. & Naqvi, S. M. Secular variations of N-isotopes in  
310 terrestrial reservoirs and ore deposits. in *Evolution of Early Earth's Atmosphere,*  
311 *Hydrosphere, and Biosphere: Constraints from Ore Deposits* 81 (2006).
- 312 7. Galloway, J. N. The Global Nitrogen Cycle. *Treatise on Geochemistry* **8**, 682 (2003).
- 313 8. Geist, D. *et al.* Hekla Revisited: Fractionation of a Magma Body at Historical  
314 Timescales. *J. Petrol.* (2021). doi:10.1093/PETROLOGY/EGAB001
- 315 9. Savage, P. S., Georg, R. B., Williams, H. M., Burton, K. W. & Halliday, A. N. Silicon  
316 isotope fractionation during magmatic differentiation. *Geochim. Cosmochim. Acta* **75**,  
317 6124–6139 (2011).
- 318 10. Sigmarsson, O., Condomines, M. & Fourcade, S. A detailed Th, Sr and O isotope study  
319 of Hekla: differentiation processes in an Icelandic Volcano. *Contrib. Mineral. Petrol.*  
320 **1992 1121** **112**, 20–34 (1992).
- 321 11. Geirsson, H. *et al.* Volcano deformation at active plate boundaries: Deep magma  
322 accumulation at Hekla volcano and plate boundary deformation in south Iceland. *J.*  
323 *Geophys. Res. Solid Earth* **117**, 11409 (2012).
- 324 12. Sigmarsson, O., Bergþórsdóttir, I. A., Devidal, J. L., Larsen, G. & Gannoun, A. Long or  
325 short silicic magma residence time beneath Hekla volcano, Iceland? *Contrib. Mineral.*  
326 *Petrol.* **177**, (2022).
- 327 13. Schuessler, J. A., Schoenberg, R. & Sigmarsson, O. Iron and lithium isotope  
328 systematics of the Hekla volcano, Iceland — Evidence for Fe isotope fractionation  
329 during magma differentiation. *Chem. Geol.* **258**, 78–91 (2009).

- 330 14. Yang, J. *et al.* Absence of molybdenum isotope fractionation during magmatic  
331 differentiation at Hekla volcano, Iceland. *Geochim. Cosmochim. Acta* **162**, 126–136  
332 (2015).
- 333 15. Prytulak, J. *et al.* Stable vanadium isotopes as a redox proxy in magmatic systems?  
334 *Geochemical Perspect. Lett.* **3**, 75–84 (2017).
- 335 16. Prytulak, J. *et al.* Thallium elemental behavior and stable isotope fractionation during  
336 magmatic processes. *Chem. Geol.* **448**, 71–83 (2017).
- 337 17. Tuller-Ross, B., Savage, P. S., Chen, H. & Wang, K. Potassium isotope fractionation  
338 during magmatic differentiation of basalt to rhyolite. *Chem. Geol.* **525**, 37–45 (2019).
- 339 18. Chen, H., Savage, P. S., Teng, F. Z., Helz, R. T. & Moynier, F. Zinc isotope fractionation  
340 during magmatic differentiation and the isotopic composition of the bulk Earth. *Earth  
341 Planet. Sci. Lett.* **369–370**, 34–42 (2013).
- 342 19. Inglis, E. C. *et al.* Isotopic fractionation of zirconium during magmatic differentiation  
343 and the stable isotope composition of the silicate Earth. *Geochim. Cosmochim. Acta*  
344 **250**, 311–323 (2019).
- 345 20. Chekol, T. A., Kobayashi, K., Yokoyama, T., Sakaguchi, C. & Nakamura, E. Timescales of  
346 magma differentiation from basalt to andesite beneath Hekla Volcano, Iceland:  
347 Constraints from U-series disequilibria in lavas from the last quarter-millennium  
348 flows. *Geochim. Cosmochim. Acta* **75**, 256–283 (2011).
- 349 21. Boocock, T. J. *et al.* Nitrogen Mass Fraction and Stable Isotope Ratios for Fourteen  
350 Geological Reference Materials: Evaluating the Applicability of Elemental Analyser  
351 Versus Sealed Tube Combustion Methods. *Geostand. Geoanalytical Res.* **44**, 537–551  
352 (2020).
- 353 22. Mikhail, S. & Sverjensky, D. A. Nitrogen speciation in upper mantle fluids and the  
354 origin of Earth’s nitrogen-rich atmosphere. *Nat. Geosci.* **7**, 816–819 (2014).
- 355 23. Jackson, C. R. M., Cottrell, E. & Andrews, B. Warm and oxidizing slabs limit ingassing  
356 efficiency of nitrogen to the mantle. *Earth Planet. Sci. Lett.* **553**, 116615 (2021).
- 357 24. Mysen, B. Nitrogen in the Earth: abundance and transport. *Prog. Earth Planet. Sci.*  
358 *2019 61* **6**, 1–15 (2019).
- 359 25. Halldórsson, S. A., Hilton, D. R., Barry, P. H., Füre, E. & Grönvold, K. Recycling of crustal  
360 material by the Iceland mantle plume: New evidence from nitrogen elemental and  
361 isotope systematics of subglacial basalts. *Geochim. Cosmochim. Acta* **176**, 206–226  
362 (2016).
- 363 26. Cartigny, P., Jendrzewski, N., Pineau, F., Petit, E. & Javoy, M. Volatile (C, N, Ar)  
364 variability in MORB and the respective roles of mantle source heterogeneity and  
365 degassing: the case of the Southwest Indian Ridge. *Earth Planet. Sci. Lett.* **194**, 241–  
366 257 (2001).
- 367 27. Busigny, V., Cartigny, P., Philippot, P., Ader, M. & Javoy, M. Massive recycling of  
368 nitrogen and other fluid-mobile elements (K, Rb, Cs, H) in a cold slab environment:  
369 evidence from HP to UHP oceanic metasediments of the Schistes Lustrés nappe

- 370 (western Alps, Europe). *Earth Planet. Sci. Lett.* **215**, 27–42 (2003).
- 371 28. Yokochi, R., Marty, B., Chazot, G. & Burnard, P. Nitrogen in peridotite xenoliths:  
372 Lithophile behavior and magmatic isotope fractionation. *Geochim. Cosmochim. Acta*  
373 **73**, 4843–4861 (2009).
- 374 29. Li, Y., Huang, R., Wiedenbeck, M. & Keppler, H. Nitrogen distribution between  
375 aqueous fluids and silicate melts. *Earth Planet. Sci. Lett.* **411**, 218–228 (2015).
- 376 30. Bucholz, C. E., Jagoutz, O., VanTongeren, J. A., Setera, J. & Wang, Z. Oxygen isotope  
377 trajectories of crystallizing melts: Insights from modeling and the plutonic record.  
378 *Geochim. Cosmochim. Acta* **207**, 154–184 (2017).
- 379 31. Li, Y., Li, L. & Wu, Z. First-principles calculations of equilibrium nitrogen isotope  
380 fractionations among aqueous ammonium, silicate minerals and salts. *Geochim.*  
381 *Cosmochim. Acta* **297**, 220–232 (2021).
- 382 32. Haendel, D., Muehle, K., Nitzsche, H.-M., Stiehl, G. & Wand, U. Isotopic variations of  
383 the fixed nitrogen in metamorphic rocks. *Geochim. Cosmochim. Acta* **50**, 749–758  
384 (1986).
- 385 33. Fischer, T. P., Takahata, N., Sano, Y., Sumino, H. & Hilton, D. R. Nitrogen isotopes of  
386 the mantle: Insights from mineral separates. *Geophys. Res. Lett.* **32**, 1–5 (2005).
- 387 34. Rudnick, R., and Gao, S., (2003) The Composition of the continental crust. In: Holland,  
388 H. D. & Turekian, K. K., Eds, Treatise on Geochemistry, Vol. 3, *The Crust*, Elsevier-  
389 Pergamon, Oxford, 1–64.
- 390 35. Taylor, S. R. Abundance of chemical elements in the continental crust: a new table.  
391 *Geochim. Cosmochim. Acta* **28**, 1273–1285 (1964).
- 392 36. McDonough, W. F., Sun, S., Ringwood, A. E., Jagoutz, E. & Hofmann, A. W. Potassium,  
393 rubidium, and cesium in the Earth and Moon and the evolution of the mantle of the  
394 Earth. *Geochim. Cosmochim. Acta* **56**, 1001–1012 (1992).
- 395 37. Marty, B. Nitrogen content of the mantle inferred from N<sub>2</sub>–Ar correlation in oceanic  
396 basalts. *Nat.* 1995 3776547 **377**, 326–329 (1995).
- 397 38. Gruber, N. & Galloway, J. N. An Earth-system perspective of the global nitrogen cycle.  
398 *Nature* **451**, 293–296 (2008).

## 399 **Methods**

400 All samples were collected, cut, cleaned and powdered during previous  
401 investigations<sup>9</sup>. In this study, the powders were cleaned once again to ensure removal of any  
402 modern surficial contaminants that may have accumulated during transport and storage. This  
403 was done by sequential washing and agitation with 18 MΩ·cm<sup>-1</sup> DI-water and methanol  
404 (reagent grade) for 1 minute each step. A centrifuge was used to remove the liquids with no  
405 observed loss of fine powdered material. Samples were subsequently dried for 48 hrs in an  
406 oven at 70 °C and stored in pre-cleaned glass scintillation vials ready for analysis.

407 Nitrogen abundances and isotope values were obtained via a custom-built  
408 combustion and tube cracker system<sup>21</sup>, optimised for accurate isotopic analyses of silicate

409 materials with low nitrogen abundances ( $< 10 \mu\text{g/g}$ ). This stainless-steel gas line is coupled to  
410 a Thermo MAT-253 isotope ratio mass spectrometer via a ConFlo IV and operates under  
411 continuous helium flow (50 ml/min). All reagents are pre cleaned via combustion at 800-1000  
412 °C for at least 6 hrs to ensure that any adsorbed  $\text{N}_2$  impurities are liberated. Exact procedural  
413 steps can be found in ref <sup>21</sup>. Approximately 300-500 mg of sample powder were weighed into  
414 the base of quartz glass tubing, using a glass thistle funnel. Around 1.0-1.1g CuO wire were  
415 also added. Sample tubes were attached to a custom-built vacuum manifold and left to  
416 evacuate to  $< 10^{-6}$  mbar overnight. The base of the sample tubes was heated to ca.150°C at  
417 this stage to remove any remaining moisture and volatile contaminants from the powders.  
418 Tubes were then sealed and removed using an oxy-propane blow-torch. The sealed evacuated  
419 sample tubes, containing the sample powder, were then placed into a muffle furnace.  
420 Samples were combusted at 1050°C for 4 hrs followed by a controlled cooling step to 600°C  
421 for 2 hrs and subsequent cooling to room temperature. This liberates all silicate bound  
422 nitrogen into gaseous form. The CuO reagent acts as both the oxygen source and acceptor  
423 preventing the formation of  $\text{NO}_x$  gases and enabling total liberation as  $\text{N}_2$  gas from the sample.  
424 These gas samples were purified and analysed using an on-line tube cracker gas line operating  
425 under continuous helium flow through a ConFlo IV into the MAT-253 IRMS. All analyses were  
426 calibrated with USGS-61 and USGS-62 Caffeine international reference materials. Procedural  
427 blanks were measured throughout the analytical campaign and had an average composition  
428 of  $22.3 \pm 3.8$  nmol total nitrogen with a  $\delta^{15}\text{N}$  value of  $-1.3 \pm 1.6$  ‰. This average analytical  
429 blank was subtracted from all standard and sample data and generally represented  $<20\%$  of  
430 the sample peak area. To assess analytical accuracy, we analysed four aliquots of BHVO-2  
431 Basalt and obtained an isotopic value of  $1.9 \pm 0.2$  ‰ and a total nitrogen abundance of  $20.2$   
432  $\pm 1.4 \mu\text{g/g}$ , which agrees well with previous studies <sup>21,39</sup>. We also measured analysed four  
433 aliquots of FKN Feldspar (CRPG) and obtained an isotopic value of  $4.2 \pm 0.5$  ‰ and a total  
434 nitrogen abundance of  $10.6 \pm 2.2 \mu\text{g/g}$ , which similarly agrees very well with previous work<sup>21</sup>.  
435 These standard data are reported in the supplementary material (Table S1).

436 Oxygen isotopes on bulk rock samples were obtained via conventional laser fluorination at  
437 the Scottish Universities Environmental Research Centre (SUERC)<sup>40</sup>. Around 2mg of powder  
438 were weighed into the sample holder. Samples were heated using a  $\text{CO}_2$  laser in the presence  
439 of  $\text{ClF}_3$  gas. Oxygen is converted to  $\text{CO}_2$  using a heated graphite rod. Replicate analyses of  
440 standards UWG2 Garnet, GP147 Garnet and YP2 Quartz were within 0.35‰ (2 s.d.) of  
441 accepted values. Data are reported using the conventional delta notation ( $\delta^{18}\text{O}$  [‰] =  
442  $[(^{18}\text{O}/^{16}\text{O}_{\text{sample}}/^{18}\text{O}/^{16}\text{O}_{\text{standard}}) - 1] \times 1000$ ) relative to the Vienna Standard Mean Ocean Water  
443 (V-SMOW). Quantitative yields to confirm the total liberation of oxygen were determined via  
444 a calibrated gas manometer. No samples were discarded for low gas yields.

445 Carbon abundances were obtained to determine if the unexplained enrichment of sample 21-  
446 09 was organic in nature. These abundances were obtained via an Elemental Analyser isolink  
447 system coupled to the same ConFlo IV and MAT253 isotope ratio mass spectrometer as the  
448 nitrogen measurements. Approximately 20mg of powdered rock samples were weighed into  
449 tin capsules for flash combustion following routine protocols<sup>41</sup>. International reference  
450 materials USGS-40 and USGS-41 were used for calibration. Measured sample peak areas were  
451 on the order of 6.0-13.4Vs with an average analytical blank of 2.6Vs.

452 **Method-only references**

- 453 39. Feng, L., Li, H. & Liu, W. Nitrogen Mass Fraction and Isotope Determinations in  
454 Geological Reference Materials Using Sealed-Tube Combustion Coupled with  
455 Continuous-Flow Isotope-Ratio Mass Spectrometry. *Geostand. Geoanalytical Res.* **42**,  
456 539–548 (2018).
- 457 40. Sharp, Z. A laser-based microanalytical method for the in situ determination of  
458 oxygen isotope ratios of silicates and oxides. *Geochim. Cosmochim. Acta* **54**, 1353–  
459 1357 (1990).
- 460 41. Stüeken, E. E., Boocock, T. J., Robinson, A., Mikhail, S. & Johnson, B. W. Hydrothermal  
461 recycling of sedimentary ammonium into oceanic crust and the Archean ocean at  
462 3.24 Ga. *Geology* **49**, 822–826 (2021).

463 **Data Availability Statement:**

464 All supporting data for this study is included in the extended data files associated with this  
465 manuscript and is deposited in a figshare repository which can be accessed through the  
466 following|:

467  
468 <https://doi.org/10.6084/m9.figshare.22242517>

469

470 **Figure Captions**

471 **Figure 1 a) Compilation of Earth reservoir size estimates for nitrogen<sup>4,5-7</sup>.** BSE = Bulk Silicate Earth. Typical  
472 nitrogen concentrations for each reservoir are shown in black above the estimates. The crust represents the  
473 third largest nitrogen reservoir and contains multiple orders of magnitude more nitrogen than the dynamic short  
474 term biological nitrogen cycle. This estimate represents total crust, including continental and oceanic crust. **b)**  
475 Compilation of felsic igneous nitrogen abundance data filtered to SiO<sub>2</sub> >60% to represent typical upper  
476 continental crust. Underlying data and associated references can be found in extended data files.

477 **Figure 2 Nitrogen abundance and isotope systematics for the Hekla volcanic suite a)** Total Alkali Silica diagram  
478 for Hekla samples measured in this study compared with literature data<sup>9, 8,10,13,20</sup>. **b)** Measured nitrogen  
479 abundances compared with Rb and Cs concentrations<sup>9</sup> plotted against barium as a highly incompatible trace  
480 element which systematically increases as the system differentiates. Nitrogen data represent average of 2-4  
481 replicate analyses with error bars representing one standard deviation around the mean. Similar partitioning  
482 behaviour is observed for nitrogen when compared with the large ion lithophile elements (Rb and Cs). Fractional  
483 crystallisation models for Rb, Cs and N, assuming a partition coefficient  $\ll 1$  ( $D_{\text{mineral-melt}} = 0.001$ , see  
484 supplemental material, Fig.S3-4). Note that sample 21-09 likely reflects some localised enrichment perhaps  
485 involving organic matter (also see supplementary material, Fig.S5). **c)** Nitrogen isotope ( $\delta^{15}\text{N}$ ) values compared  
486 with the Icelandic mantle plume<sup>25</sup>, atmospheric air (defined as  $\delta^{15}\text{N} = 0.0$ ) and average convecting upper mantle  
487 (i.e., MORB)<sup>26</sup>. **d)** Molar N/Rb ratio versus silica showing a general constancy across the differentiation suite.  
488 N/Rb values for subducting slab sediments/altered oceanic crust<sup>27</sup> and the lithospheric mantle<sup>28</sup> are highlighted.  
489 The constancy of N/Rb ratio indicates a similar behaviour between nitrogen and rubidium during magmatic  
490 differentiation. Were nitrogen degassing (fluid-melt  $D_{\text{N}} = 60\text{-}10000$ )<sup>29</sup> and Rb behaving incompatibly ( $D_{\text{Rb}} = 0.001$ )  
491 the N/Rb ratio would decrease rapidly, which is not observed by our data. Modelled lines show predicted N/Rb  
492 variations if a fraction of the total silicate nitrogen was degassing (0%, 1%, 5% and 100%) calculated using the  
493 most conservative fluid-melt  $D_{\text{N}} = 60$  (measured on felsic compositions). This is a maximum estimate as it is likely

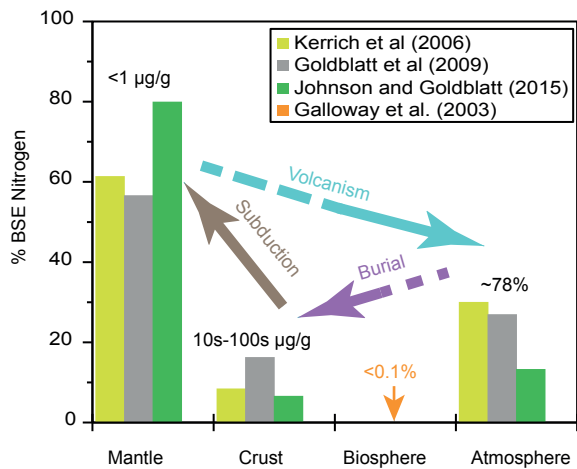
494 more appropriate to use the fluid-melt  $D_N = 10,000$  (measured on basaltic compositions) which suggest only  
495 0.006-0.03% of nitrogen can have degassed.

496 **Figure 3 Nitrogen versus rubidium for the Hekla suite and fractional crystallisation model.** Rubidium contents  
497 of the Middle Continental Crust (MCC) of  $65 \pm 4 \mu\text{g/g}$  and Upper Continental Crust (UCC) of  $84 \pm 17 \mu\text{g/g}$  taken  
498 from ref <sup>34</sup> and propagated up to the modelled fractional crystallisation lines. White dotted line represents the  
499 mean value, with shaded grey/pink bars the one standard deviation on the mean for this estimate. Nitrogen  
500 error bars represent the standard deviation of the mean value of between 2-4 replicate analyses of each sample.

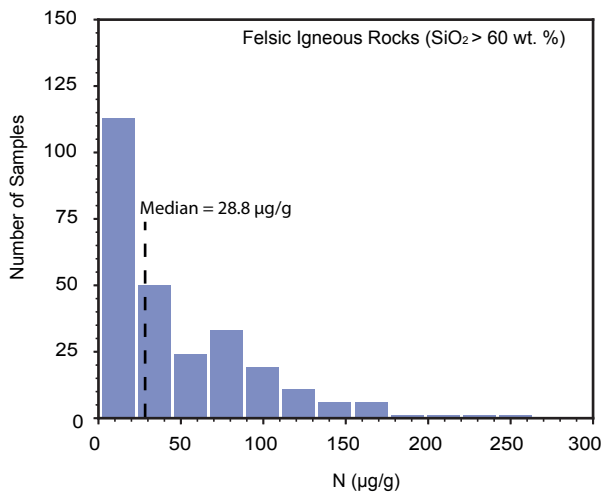
501



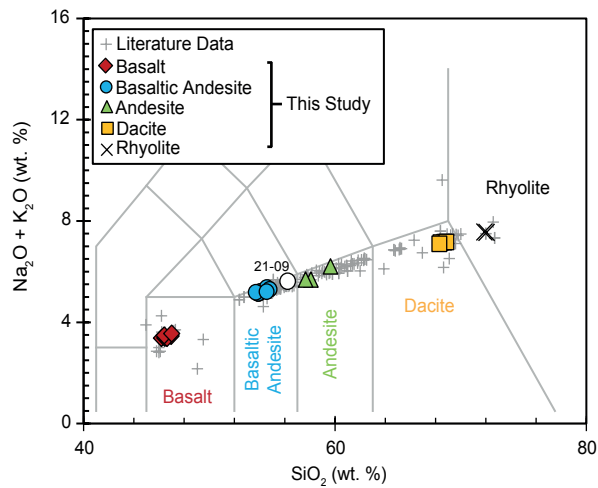
a



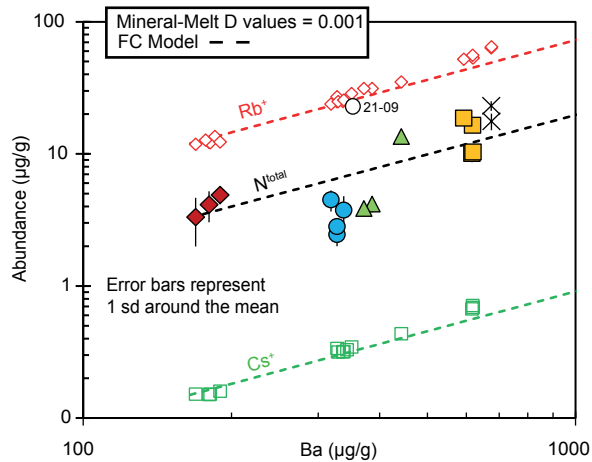
b



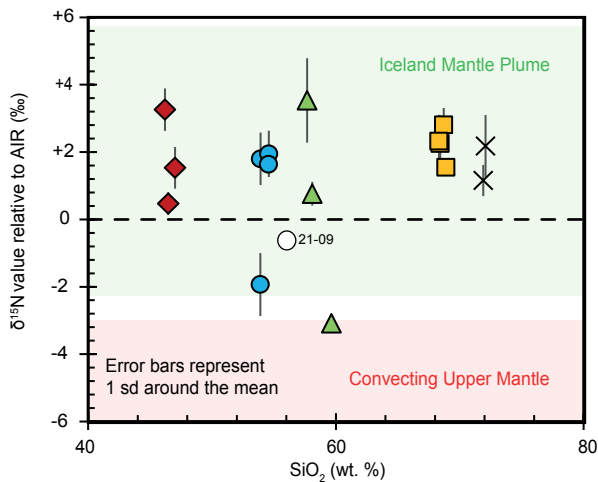
a



b



c



d

